Boletim da Sociedade Astronômica Brasileira, **35**, no. 1, 160-164

Rotation–magnetic activity relation for late-F, G, K, and M stars

L. J. Galvão[1], N. R. Landin[2], & S. H. P. Alencar[1]

[1] Departamento de Física, Universidade Federal de Minas Gerais, Belo Horizonte, Brazil.
e-mail: lucasgj@ufmg.br, silvia@fisica.ufmg.br
[2] Universidade Federal de Viçosa, campus UFV Florestal. e-mail: nlandin@ufv.br

Abstract. The study of the rotation–magnetic activity relation helps us to understand the physical processes that occur in stellar interiors. Observational data indicate that magnetic activity is correlated with the Rossby number, *Ro*. In this work, we investigate the relation between two magnetic activity indicators, the fractional X–ray luminosity, L_X/L_{bol}, and the average large–scale surface magnetic field $\langle|B_V|\rangle$, and the Rossby number. *Ro* was calculated using models generated by the stellar evolution code ATON. This relationship between magnetic activity indicators and the Rossby number can be expressed by a saturated region, where $Ro \leq Ro_{sat}$ and an unsaturated region, where the magnetic activity indicator decreases in a power—law dependence with increasing Ro described by a power—law slope β. The average magnetic activity indicators in the saturation regime are defined as $(L_X/L_{bol})_{sat}$ and $\langle|B_V|\rangle_{sat}$. Aiming to analyze the rotation–magnetic activity relationship for low-mass stars, we choose a sample of 73 late–F, G, K, and M dwarf stars, in the main sequence and pre-main sequence phases. We put the data in the rotation–magnetic activity diagram and analyzed them using a Markov Chain Monte Carlo (MCMC) method. Finally, we find $(L_X/L_{bol})_{sat} = (0.77 \pm 0.01) \times 10^{-3}$, $Ro_{sat} = 0.045 \pm 0.002$ and $\beta = -1.29 \pm 0.08$ using the fractional X–ray luminosity as a magnetic activity indicator and $\langle|B_V|\rangle_{sat} = (155 \pm 5)$ G, $Ro_{sat} = 0.059 \pm 0.002$ and $\beta = -1.23 \pm 0.01$ using the average large–scale surface magnetic field as such.

Resumo. O estudo da relação rotação–atividade magnética nos ajuda a entender os processos físicos que ocorrem nos interiores estelares. Dados observacionais indicam que a atividade magnética é correlacionada com o número de Rossby, *Ro*. Neste trabalho, investigamos a relação entre dois indicadores de atividade magnética, a luminosidade fracionária em raios–X, L_X/L_{bol}, e a média do campo magnético superficial em larga escala, $\langle|B_V|\rangle$, e o número de Rossby. *Ro* foi calculado usando modelos gerados pelo código de evolução estelar ATON. Essa relação entre os indicadores de atividade magnética e o número de Rossby pode ser expressa por uma região saturada, onde $Ro \leq Ro_{sat}$ e uma região insaturada, onde o indicador de atividade magnética diminui em uma dependência da lei de potência com o aumento de Ro descrito por uma inclinação da lei de potência β. Os indicadores médios de atividade magnética no regime de saturação são definidos como $(L_X/L_{bol})_{sat}$ e $\langle|B_V|\rangle_{sat}$. Com o objetivo de analisar a relação rotação–atividade magnética para estrelas de baixa massa, escolhemos uma amostra de 73 estrelas anãs do tipo tardio–F, G, K e M, na sequência principal e pré-sequência principal. Os dados foram colocados no diagrama rotação–atividade magnética e analisados com um método de Monte Carlo via Cadeias de Markov (MCMC). Por fim, encontramos $(L_X/L_{bol})_{sat} = (0.77 \pm 0.01) \times 10^{-3}$, $Ro_{sat} = 0.045 \pm 0.002$ e $\beta = -1.29 \pm 0.08$ usando L_X/L_{bol} como indicador de atividade magnética e $\langle|B_V|\rangle_{sat} = (155 \pm 4)$ G, $Ro_{sat} = 0.059 \pm 0.002$ e $\beta = -1.23 \pm 0.01$ usando a média do campo magnético superficial em larga escala como tal.

Keywords. stars: activity – stars: low-mass – stars: rotation

1. Introduction

There are many old records of naked–eye observations of spots on the Sun surface. These reports are found in different cultures, such as Chinese and Korean, and can be used to understand the cycle of magnetic activity in our Sun (Chol-jun & Jik-su 2020). Naked-eye observations are used, for example, to describe the Maunder Minimum, a period of low solar activity (Wang & Li 2022).

Spots are an important manifestation of magnetic activity in stars, but they are not the only ones. Other examples of such indicators are the large–scale surface magnetic fields, the coronal X-ray emission and the Hα and CaII chromospheric emissions. The magnetic activity is connected to stellar rotation and was initially analyzed as a function of the stellar rotation period (P_{rot}). The dependence of magnetic activity on the Rossby number, defined as the ratio between P_{rot} and the convective turnover time, τ_c, was first investigated by Noyes et al. (1984). τ_c is a characteristic variable of the Mixing Length Theory (MLT) and is described as the ratio between the mixing length (ℓ) and the convective velocity v_c. Convective mixing length is the characteristic length scale of convection in which an element of mass moves until dissipating in the surroundings.

τ_c can be obtained by two different methods: a semiempiric one, in which τ_c is estimated as a function of a color index and a theoretical one, in which it is calculated by stellar evolution models. To determine the turnover convective time, Noyes et al. (1984) and Pizzolato et al. (2003) utilized τ as a function of $B-V$. Cranmer & Saar (2011) describe τ_c as a function of effective temperature for stars in the range 3300 K $\lesssim T_{eff} \lesssim$ 7000 K. Wright et al. (2011) used $\tau_c(B-V)$ and $\tau_c(V-K)$. Landin, Mendes, & Vaz (2010) determinated theoretical values of τ_c for solar–like stars in the pre–main sequence using the ATON 2.3 stellar evolutionary code.

For a specific age and mass, convective turnover times vary with radius. For partially convective stars, τ_c is usually calculated at one half of a mixing length above the base of the convective zone (Noyes et al. 1984). However, this prescription is inadequate for fully convective stars because they do not have a tachocline (a thin shear layer between the radiative core and the convective envelope). For these stars, we can calculate τ_c at a different place, related to the pressure scale height, as proposed by Landin et al. (2023).

The study of the relation between magnetic–activity and rotation in general is made through rotation–magnetic activity diagrams, such as plots of L_X/L_{bol} (fractional X–ray luminosity) and $\langle|B_V|\rangle$ (unsigned average large–scale surface magnetic

field strength) as a function of *Ro*. The rotation–magnetic activity diagrams are characterized by two regions delimited by a threshold value of *Ro* named saturated Rossby number, $Ro_{\rm sat}$. For $Ro \leq Ro_{\rm sat}$, $L_{\rm X}/L_{\rm bol}$ and $\langle|B_V|\rangle$ do not depend on *Ro* (saturated region). In the description of magnetic–activity, a value of saturation for this region is defined as $(L_{\rm X}/L_{\rm bol})_{\rm sat}$ or $\langle|B_V|\rangle_{\rm sat}$. For $Ro > Ro_{\rm sat}$ (unsaturated region), $L_{\rm X}/L_{\rm bol}$ and $\langle|B_V|\rangle$ decrease with increasing *Ro* described by a power–law with slope β.

Alexander & Preibisch (2012) studied young stars from the IC 348 cluster (age $\approx$ 3 Myr). With $L_{\rm X}/L_{\rm bol}$ from Chandra observations and *Ro* determined with stellar models, they observed that all stars from their sample were in a saturated regime of magnetic–activity. For rapid rotators ($Ro < 0.006$), Alexander & Preibisch (2012) found evidence of a super–saturation regime. For the saturated regime and super–saturated regime, the average values of fractional X–ray luminosity they obtained were $\log(L_{\rm X}/L_{\rm bol}) = -3.51$ and $\log(L_{\rm X}/L_{\rm bol}) = -3.56$, respectively. With a compiled sample of G, K and M–type stars from the literature and semi–empirical convective turnover times, Wright et al. (2011) found $\log(L_{\rm X}/L_{\rm bol})_{\rm sat} = -3.13 \pm 0.08$, $Ro_{\rm sat} = 0.13 \pm 0.02$ and $\beta = -2.18 \pm 0.16$. For a sample with fully convective stars in the unsaturated regime of magnetic activity and convective turnover times calculated using the observed values of $V - K$ and the $\tau(V - K)$ relation from Wright et al. (2011), Wright et al. (2018) obtained $\log(L_{\rm X}/L_{\rm bol})_{\rm sat} = -3.05^{+0.05}_{-0.06}$, $Ro_{\rm sat} = 0.14^{+0.08}_{-0.04}$ and $\beta = -2.3^{+0.4}_{-0.6}$. Furthermore, for a sample of 73 stars with convective turnover times calculated theoretically, Vidotto et al. (2014) found $\beta = -1.38 \pm 0.14$ for $Ro \gtrsim 0.1$ and $\langle|B_V|\rangle_{\rm sat} = 50$ G (for early M dwarfs) and $\langle|B_V|\rangle_{\rm sat} = 398$ G (for mid M dwarfs) for the saturated regime. Using a sample of 85 low-mass stars and convective turnover times calculated as a function of effective temperatures described in Cranmer & Saar (2011), See et al. (2019) obtained $\langle|B_V|\rangle_{\rm sat} = 257 \pm 72$, $Ro_{\rm sat} = 0.06 \pm 0.01$ and $\beta = -1.40 \pm 0.10$.

The objective of this work is to investigate the rotation–magnetic activity relation using τ_c calculated theoretically with the method proposed by Landin et al. (2023). To accomplish this, we used the sample of 73 late-F, G, K, and M dwarf stars from Vidotto et al. (2014). We investigated the dependence between magnetic–activity and age through the rotation–magnetic activity diagram for $L_{\rm X}/L_{\rm bol}$ x *Ro* and $\langle|B_V|\rangle$ x *Ro*. In addition, with the aim of describing the data in the diagram, we used a Markov Chain Monte Carlo (MCMC) resampling method to determine $(L_{\rm X}/L_{\rm bol})_{\rm sat}$, $\langle|B_V|\rangle_{\rm sat}$, $Ro_{\rm sat}$ and β.

In Sec. 2, we describe the stellar models used in this work. In Sec. 3 we present the sample of stars and the source of observational parameters. The discussion about the calculation of τ_c and *Ro* and the effect of age on the rotation–magnetic activity diagram is in Sec. 4. In Sec. 5, we outline the determination of parameters that describe the rotation–magnetic activity diagram by the MCMC method and discuss our results. In Sec. 6, we present our conclusions.

2. Models

We use the evolutionary tracks generated by the ATON code with solar metallicity, as described by Asplund et al. (2009). We assume differential rotation and the initial angular momentum described by the relation $J_{\rm Kaw} = 1.566 \times 10^{50} (M/{\rm M}_\odot)^{0.985}$ g cm^2 s^{-1} from Kawaler (1987). We use the Mixing Length Theory by Böhm-Vitense (1958) to treat convection, with the parameter α related to the convection efficiency fixed at $\alpha = 2.0$. The adjustment between the interior and the atmosphere was done at the optical depth $\tau = 3$ and the surface boundary conditions were obtained from non-gray atmosphere models (Allard, Hauschildt & Schweitzer 2000).

3. The sample of stars

In this work we used the sample of 73 late–F, G, K, and M dwarf stars from Vidotto et al. (2014). This sample is composed of solar–like stars (spectral types F, G and K) with ages $\geq$ 260 Myr, young solar–like stars with ages between 35 Myr and 130 Myr and M dwarf stars (with ages between 21 Myr and 1200 Myr). The maximum and minimum magnetic–activity of the Sun was also considered. Additionally, the sample includes young low–mass accreting stars (Classical T Tauri stars) and hot–Jupiter hosts. Rotation periods, the fractional X–ray luminosity and the average large–scale surface magnetic field, reconstructed using the ZDI technique, come from Vidotto et al. (2014). The mass and age of the sample are from Vidotto et al. (2014), except for 12 M dwarfs and one T Tauri star without determined ages. For these stars, we calculate the age using the ATON code (Landin et al. 2023). For the T Tauri star, we used the lower age limit from Hussain et al. (2009). More details are in Landin et al. (in preparation).

4. *Ro* determination and the rotation–magnetic activity diagram

We used the method described by Landin et al. (2023), based on theoretical results obtained with the ATON code, to determine τ_c for the stars in our sample. This method consists of expressing the location where τ_c is usually calculated for partially convective stars (one half of a mixing length above the base of the convective zone) in terms of the pressure scale height, making a linear fit of this position as a function of stellar mass and extrapolating it to fully convective stars ($M < 0.4\ M_\odot$). Using these theoretical convective turnover times, Rossby numbers were calculated with the rotation periods from Vidotto et al. (2014) and rotation–magnetic activity diagrams were obtained using the fractional X–ray luminosity and the average large-scale surface magnetic field also from Vidotto et al. (2014). Our results are shown in Fig. 1. In both panels, the color bars indicate the age of the stars. It is possible to see that older stars are in the unsaturated region in rotation magnetic–activity diagrams, while younger stars are in the magnetic activity saturation regime. The decrease of magnetic activity as a function of age in both diagrams is consistent with what Vidotto et al. (2014) and Folsom et al. (2018) found.

Fig. 1 shows that the dispersion in the saturated region of $\langle|B_V|\rangle$ x *Ro* is more significant than for $L_{\rm X}/L_{\rm bol}$. This is because $L_{\rm X}/L_{\rm bol}$ is sensible to all magnetic energies, while $\langle|B_V|\rangle$ is sensible only to the magnetic energy associated with large–scale fields. For $M \sim 0.4$ M$_\odot$, the large–scale field has an abrupt variation and is slightly larger for mid–M stars than for early–Ms (Donati et al. 2008).

5. Determination of $(L_{\rm X}/L_{\rm bol})_{\rm sat}$, $\langle|B_V|\rangle_{\rm sat}$, $Ro_{\rm sat}$ and β

To fit the three parameters of the rotation–magnetic activity relationship described in Eqs. 1 and 2 below, we used the Markov Chain Monte Carlo resampling method, as implemented in the open source package *emcee.py* in Python (Foreman-Mackey et al. 2013). To run the code, it is necessary to define the model which is supposed to describe the data in the rotation–magnetic

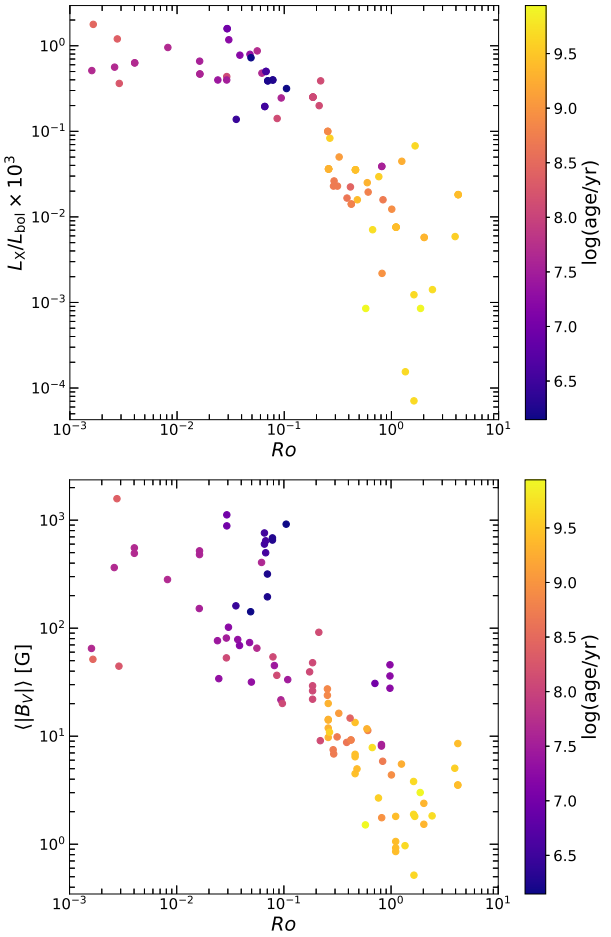

Figure 1. Top: L_X/L_{bol} x Ro. Bottom: $\langle|B_V|\rangle$ x Ro for our sample. Adapted from Vidotto et al. (2014).

activity diagram. The input functions used in the MCMC code were two–part power–laws:

$$L_X/L_{bol} = \begin{cases} CRo^{\beta}, & \text{if } Ro > Ro_{sat}, \\ (L_X/L_{bol})_{sat}, & \text{if } Ro \leq Ro_{sat}, \end{cases} \quad (1)$$

$$\langle|B_V|\rangle = \begin{cases} CRo^{\beta}, & \text{if } Ro > Ro_{sat}, \\ \langle|B_V|\rangle_{sat}, & \text{if } Ro \leq Ro_{sat}, \end{cases} \quad (2)$$

where $(L_X/L_{bol})_{sat}$ and $\langle|B_V|\rangle_{sat}$ are the average values of the parameters in the saturated regions, β is the inclination of the unsaturated region (in a log-log scale) and C is a constant: $C = (L_X/L_{bol})_{sat}/{Ro_{sat}}^{\beta}$ for L_X/L_{bol} and $C = \langle|B_V|\rangle_{sat}/{Ro_{sat}}^{\beta}$ for $\langle|B_V|\rangle$, so that the functions are continuous at Ro_{sat}. We define 400 random values for each parameter within a predefined range: $30 < \langle|B_V|\rangle_{sat}/\mathrm{G} < 400$, $-2.0 < \beta < -0.5$ and $0.03 < Ro_{sat} < 0.15$ for $\langle|B_V|\rangle$ and $0.3 < (L_X/L_{bol})_{sat} \times 10^3 < 1.7$, $-2 < \beta < 0$ and $0.02 < Ro_{sat} < 0.07$ for L_X/L_{bol}. The initial parameter sets are shown in Fig. 2. Each point of this 3D parameter space is also called a walker. At each step of the chain, the walker can vary and assume new values for the three parameters. With these new values, the walker generates a model with the two–part power–law function which is compared with the data through a likelihood as:

$$L = \Pi \exp\left(-\frac{(MI_{data} - MI_{model})^2}{2\sigma^2}\right), \quad (3)$$

where MI_{data} is the magnetic–activity indicator data, MI_{model} is the model constructed with the functions described by Eqs. 1 or 2 using the walker sets as input parameters and σ^2 is the MI_{data} uncertainty. For L_X/L_{bol}, we used the errors from Vidotto et al. (2014). For $\langle|B_V|\rangle$, we considered σ as 0.05, since the values of $\langle|B_V|\rangle$ are listed with two decimal digits in Vidotto et al. (2014). The movement of walkers is ruled by an acceptance ratio, which defines whether they move or not between the steps of the chain. If the new values after a movement in the parameter space produce a better correlation between the data and the model, the walker will go to this new location of the parameter space. Otherwise, it continues with previous values. In this case, in the next step the walker examines the parameter space in another direction. As a result, the walkers explore the parameter space searching for the set of three values that maximizes the likelihood.

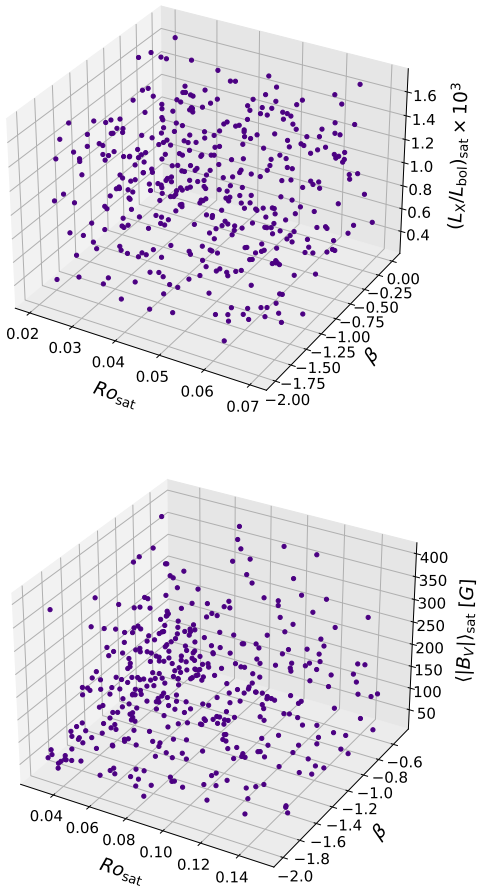

Figure 2. Parameters spaces where the initial parameters are defined for L_X/L_{bol} x Ro (top) and $\langle|B_V|\rangle$ x Ro (bottom).

In the analysis of the L_X/L_{bol} x Ro diagram, the autocorrelation times for each parameter are around 18, 23 and 26 iterations for $(L_X/L_{bol})_{sat} \times 10^3$, Ro_{sat} and β, respectively, and 22, 24 and 18 iterations for $\langle|B_V|\rangle_{sat}$, Ro_{sat} and β in the analysis of the $\langle|B_V|\rangle$ x Ro diagram. The autocorrelation time indicates the number of steps necessary for the parameters to converge to the best parameters without the influence of the initial parameters.

Time series for each parameter in the chain are presented in Fig. 3. Intending to reduce the influence of the initial set in the analysis of the posterior distribution, we discarded twice the maximum of the correlation time from initial iterations. The corner plot on Fig. 4 shows the posterior distribution of parameters for L_X/L_{bol} and $\langle|B_V|\rangle$. On the upper diagonal in each plot, we have histograms for all parameters analyzed in MCMC. The dashed lines indicate the 16th and 84th percentiles on the marginalized distributions that were used to determine the parameter errors and blue lines indicate the 50th percentile, i.e. the best-fit parameters. In the corner, we have a two-dimensional projection to show the covariance between the values.

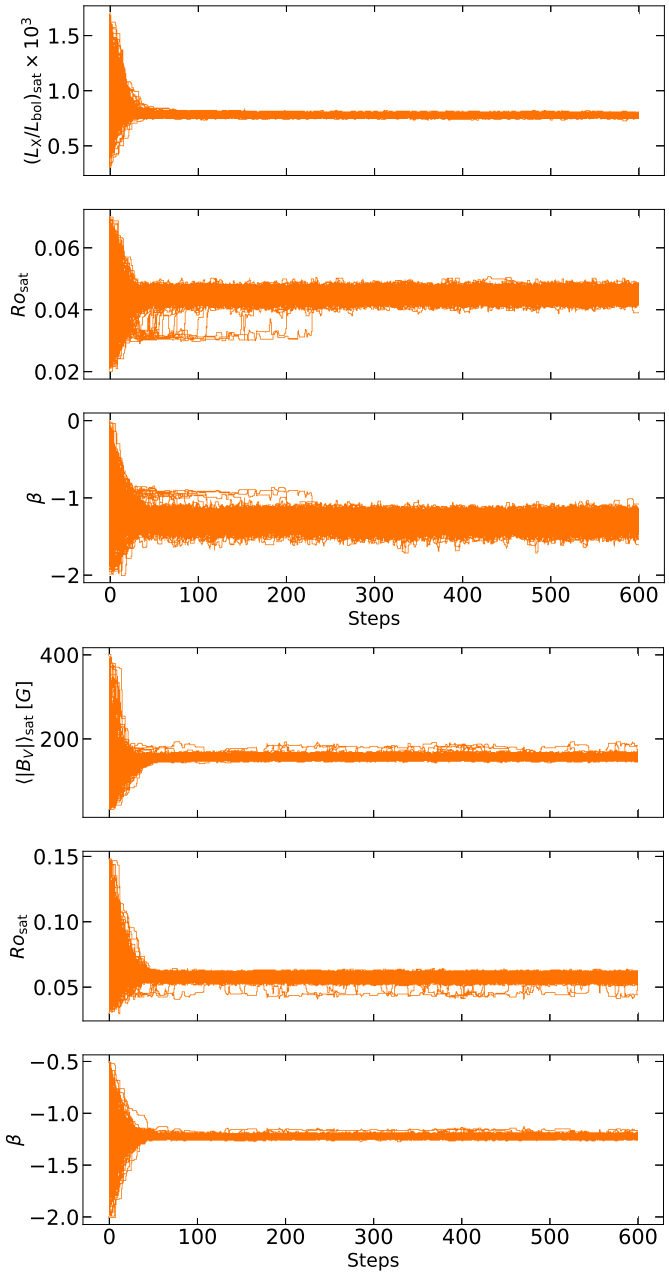

Figure 3. Time series for each parameter for L_X/L_{bol} x Ro (top) and $\langle|B_V|\rangle$ x Ro (bottom).

The resulting parameters are shown in Fig. 5 for L_X/L_{bol} x Ro and for $\langle|B_V|\rangle$ x Ro. The curves in orange correspond to 100 random draws from the posterior distribution.

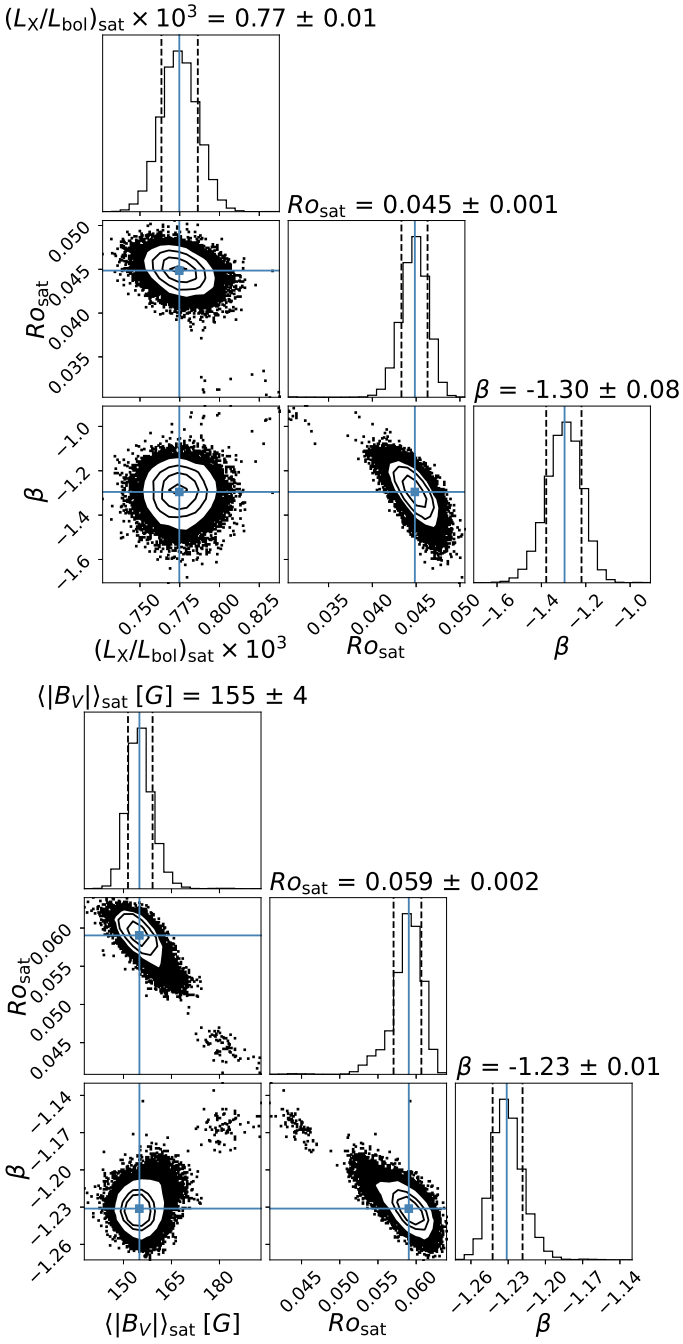

Figure 4. One-dimensional and two-dimensional projections of posterior probability distributions from the MCMC method made with *corner.py* (Foreman-Mackey 2016) for L_X/L_{bol} x Ro (top) and $\langle|B_V|\rangle$ x Ro (bottom). Contours represents 0.5σ, 1σ, 1.5σ, and 2σ.

Using this method, we find $(L_X/L_{bol})_{sat} = (0.77 \pm 0.01) \times 10^{-3}$, $Ro_{sat} = 0.045 \pm 0.002$ and $\beta = -1.29 \pm 0.08$. For the average large–scale surface magnetic field, we find $\langle|B_V|\rangle_{sat} = (155 \pm 4)$ G, $Ro_{sat} = 0.059 \pm 0.002$ and $\beta = -1.23 \pm 0.01$. The 50th, 16th and 84th percentiles on the marginalized distributions were chosen as stated values which maximize the posterior distribution of parameters, given the data, and inferior and superior uncertainties, respectively.

In Fig. 5 we can see that M dwarf stars are mostly found in the saturated regime, while T Tauri stars are found in the region

between unsaturated and saturated regimes. Young suns have relatively more emission in the L_X/L_{bol} x Ro diagram than in the $\langle|B_V|\rangle$ x Ro one, what puts them in a more unsaturated regime in the first plot. Solar–like stars are located in the unsaturated region, like the Sun. Hot–Jupiter hosts do not present an anomalous behavior in the magnetic–activity diagram, which indicates that planets' tidal forces are insufficient to generate any specific trend in the behavior of these objects in these plots, as discussed by Vidotto et al. (2014).

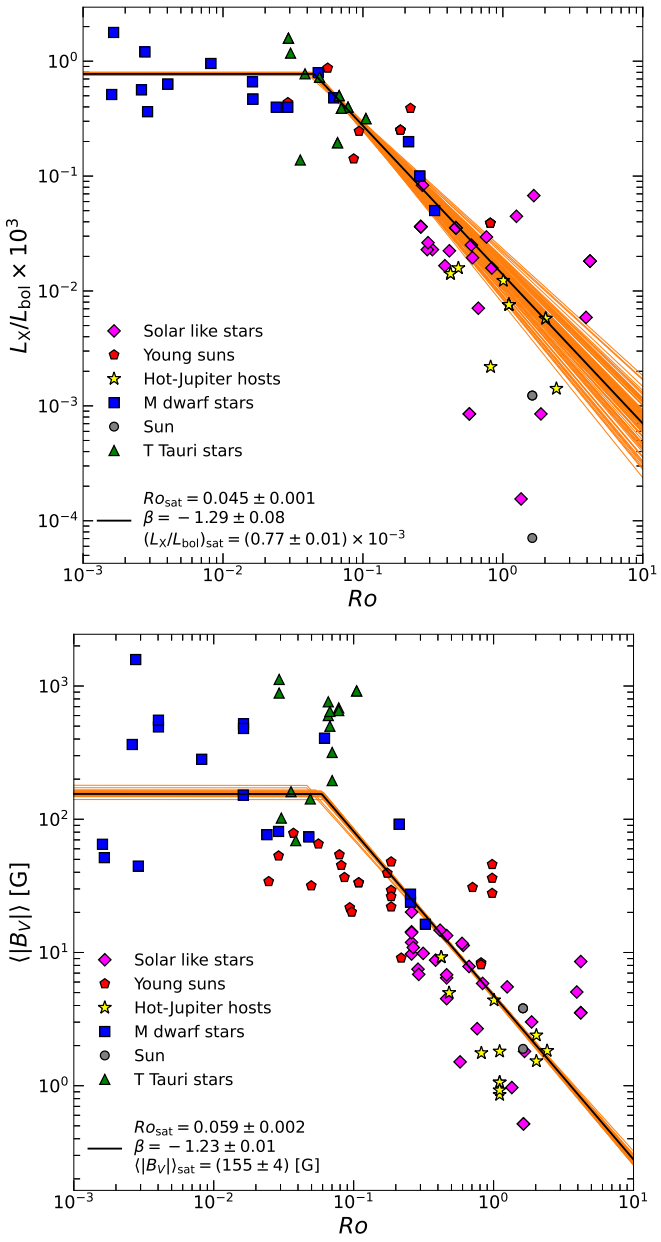

Figure 5. Top: L_X/L_{bol} x Ro. Bottom: $\langle|B_V|\rangle$ x Ro. Black lines are the model described with the best-fit parameters and straight orange lines are 100 random draws from the posterior distribution. L_X/L_{bol}, $\langle|B_V|\rangle$ and P_{rot} values come from Vidotto et al. (2014).

6. Conclusions

With a new method proposed by Landin et al. (2023) to calculate convective turnover times theoretically, it was possible to reproduce the rotation–magnetic activity relationship for the sample of late-F, G, K, and M stars from Vidotto et al. (2014). Through the rotation–magnetic activity diagram, we verified the dependency of magnetic activity as a function of age, finding the youngest stars of our sample in the saturation regime.

Using the MCMC method, we found the most likely parameters that describe the rotation–magnetic activity relation for our sample of stars. For L_X/L_{bol} x Ro, we obtained $(L_X/L_{bol})_{sat} = (0.77 \pm 0.01) \times 10^{-3}$, $Ro_{sat} = 0.045 \pm 0.002$ and $\beta = -1.29 \pm 0.08$. In addition, for $\langle|B_V|\rangle$ x Ro we found $\langle|B_V|\rangle_{sat} = (155 \pm 4)$ G, $Ro_{sat} = 0.059 \pm 0.002$ and $\beta = -1.23 \pm 0.01$. The fact that our values of Ro_{sat} and β are only marginally consistent with the values from Wright et al. (2011) and Wright et al. (2018) can be due to differences between the methods of convective turnover time determination and by the fact that our sample is smaller than theirs. Moreover, our value of $(L_X/L_{bol})_{sat}$ is not as low as that of Alexander & Preibisch (2012), whose sample is constituted of very active young stars. The determination of our parameters using MCMC and the method used to calculate τ_c can be possible answers for the difference between our $\langle|B_V|\rangle_{sat}$ and β values and those from See et al. (2019), although we have both obtained low values of Rossby number saturation when compared to the value usually accepted in the literature, $Ro \approx 0.1$ (Pizzolato et al. 2003). The difference between our parameters values in relation to those from Vidotto et al. (2014), who fit to the data with a fixed Ro_{sat}, can be due to the different fitting method used in both works.

Acknowledgments. The authors thank F. D'Antona and I. Mazzitelli (in memoriam) for allowing them to use and improve the ATON code. The Brazilian agencies CAPES, CNPq, and FAPEMIG and the graduate program in physics at UFMG are acknowledged for financial support.

References

Alexander F., Preibisch T., 2012, A&A, 539, A64.
Allard, F.; Hauschildt, P. H.; Schweitzer, A., 2000, ApJ, 539, 366.
Asplund, M.; Grevesse, N.; Sauval, A. J.; Scott, P., 2009, ARA&A, 47, 481.
Böhm-Vitense, E., 1958, Z. Astrophys., 46, 108.
Chol-jun K., Jik-su K., 2020, MNRAS, 492, 384.
Cranmer S. R., Saar S. H., 2011, ApJ, 741, 54.
Donati J.-F. et al., 2008, MNRAS, 390, 545.
Folsom C. P., Bouvier J., Petit P., Lèbre A., Amard L., Palacios A., Morin J., Donati J. -F., Vidotto A. A., 2018, MNRAS, 474, 4956.
Foreman-Mackey D., 2016, JOSS, 1, 24.
Foreman-Mackey D., Hogg D. W., Lang D., Goodman J., 2013, PASP, 125, 306.
Hussain G. A. J. et al., 2009, MNRAS, 398, 189.
Kawaler, S. D., 1987, PASP, 99, 1322.
Landin N. R., Mendes L. T. S., Vaz L. P. R., 2010, A&A, 510, A46.
Landin N. R., Mendes L. T. S., Vaz L. P. R., Alencar S. H. P., 2023, MNRAS, 519, 5304.
Noyes R. W., Hartmann L. W., Baliunas S. L., Duncan D. K., Vaughan A. H., 1984, ApJ, 279, 763.
Pizzolato N., Maggio A., Micela G., Sciortino S., Ventura P., 2003, A&A, 397, 147.
See V. et al., 2019, ApJ, 876, 118.
Vidotto, A. A. et al., 2014, MNRAS, 441, 2361.
Wang H., Li H., 2022, SoPh, 297, 127.
Wright N. J., Drake J. J., Mamajek E. E., Henry G. W., 2011, ApJ, 743, 48.
Wright N. J., Newton E. R., Williams P. K. G., Drake J. J., Yadav R. K., 2018, MNRAS, 479, 2351.